

# Q-Structure beneath the north and central Indian Ocean from the inversion of observed Love and Rayleigh wave attenuation data

D.D. Singh

National Geophysical Research Institute, Hyderabad — 500007 (A.P.) (India)

(Received November 7, 1986; revision accepted November 15, 1988)

Singh, D.D., 1990. Q-Structure beneath the north and central Indian Ocean from the inversion of observed Love and Rayleigh wave attenuation data. *Phys. Earth. Planet. Inter.*, 59: 243–258.

The fundamental-mode Love and Rayleigh waves generated by 57 earthquakes which occurred in the north and central Indian Ocean (extending to 40°S) and recorded at Indian seismograph and other WWSSN stations such as HOW, SHL, VIS, MDR, HYB, KOD, CHG, TRD, POO, BOM, GOA, NDI, NIL and QUE are analysed. Love and Rayleigh wave attenuation coefficients are estimated at periods of 15–100 s using the spectral amplitude of these waves for 98 different paths across the Bay of Bengal Fan, the Arabian Fan, and the north and central Indian Ocean. The large standard deviations observed in the surface wave attenuation coefficients may be a result of regional variation of the attenuative properties of the crust and upper mantle beneath these regions. Love wave attenuation coefficients are found to vary from 0.000 03 to 0.000 45 km<sup>-1</sup> for the Bay of Bengal Fan; from 0.000 03 to 0.000 85 km<sup>-1</sup> for the Arabian Fan; and from 0.000 03 to 0.000 35 km<sup>-1</sup> for the north and central Indian Ocean. Similarly, Rayleigh wave attenuation coefficients vary from 0.000 03 to 0.0004 km<sup>-1</sup> for the Bay of Bengal Fan; from 0.000 06 to 0.0007 km<sup>-1</sup> for the Arabian Fan; and from 0.000 03 to 0.0007 km<sup>-1</sup> for the north and central Indian Ocean. Backus and Gilbert inversion theory is applied to these surface wave attenuation data to obtain average  $Q^{-1}$  models for the crust and upper mantle beneath the Bay of Bengal, the Arabian Fan, and the north and central Indian Ocean. Inversion of Love and Rayleigh wave attenuation data shows a high-attenuation zone centred at a depth of > 120 km ( $Q_{\beta} \approx 125$ ) for the Bay of Bengal Fan. Similarly, a high-attenuation zone ( $Q_{\beta} \approx 40-70$ ) occurs at a depth of 60–160 km for the Arabian Fan at 100–160 km ( $Q_{\beta} \approx 115$ ) for the Indian Ocean off Ninetyeast Ridge, and at 80–160 km ( $Q_{\beta} \approx 80$ ) for the Indian Ocean across the Ninetyeast Ridge. The  $Q_{\beta}^{-1}$  models show a lithosphere thickness of 120 km beneath the Bay of Bengal Fan. Similarly, lithosphere thickness of 70, 100 and 80 km is estimated beneath the Arabian Fan, and the Indian Ocean off Ninetyeast Ridge and across Ninetyeast Ridge, respectively. The base of the lithosphere is identified as the depth at which there is a significant increase in the  $Q_{\beta}^{-1}$  value, which attains its maximum value in the asthenosphere. The thinning of Indian lithosphere beneath the Arabian Fan suggests high temperature below Moho depth (60 km from surface) which has caused a high-attenuation zone at this shallow depth.

## 1. Introduction

The Indian Ocean is one of the largest oceans in the world. In comparison with other oceans very few geophysical studies have been made for it, and it is of interest to discover the material condition existing in different parts of Indian Ocean by studying the regional variation of attenuation,  $Q$ . As seismic wave attenuation is more sensitive to variation in temperature and partial

melting, mapping of the  $Q$ -structure beneath various geological environments is a useful tool to delineate the lithosphere–asthenosphere boundary, which gives an important constraint for study of the mechanism of the intrusion process. The spatial variation of attenuation beneath a ridge axis or near spreading centres will give an important constraint on the crust and upper mantle temperature conditions and the process of lithosphere generation. High attenuation is associated with a

partial melting zone, and a very low  $Q$  value corresponds to a region in which the melt phase occupies most of the volume. However, surface wave attenuation measurements are subject to larger uncertainties than are velocity measurements, including variation of amplitude as a result of source geometry, departures from ideal instrumental effect, various propagation effects which include interference between modes and mode conversion, lateral refraction (McGarr, 1969) and multi-pathing (Capon, 1971) at the ocean–continent margins. The effect of source geometry is removed by considering the fault plane orientations available in these regions, and other sources of error are assumed to affect the observed attenuation data in a random way. In that case, they would be reflected in the confidence limits for the observations but would not systematically affect the observations. In certain cases, however, these factors may also cause our observed attenuation values to be systematically high or low without affecting their confidence limits. Such a situation can be improved by considering a large number of data sets for the same path. Mitchell (1975) observed systematically low attenuation coefficients at certain periods which were associated with regional variations in the anelastic properties of the crust of North America. We have analysed the fundamental-mode Love and Rayleigh waves generated by 57 earthquakes which occurred in the north and central Indian Ocean (extending to  $40^\circ\text{S}$ ) and recorded at the eastern and western margins of the Indian subcontinent by Indian Seismograph and other World Wide Standard Seismograph Network (WWSSN) stations such as Howrah (HOW), Shillong (SHL), Vishakhapatnam (VIS), Madras (MDR), Hyderabad (HYB), Kodaikanal (KOD), Chiangmai (CHG), Trivandrum (TRD), Poona (POO), Bombay (BOM), Goa (GOA), New Delhi (NDI), Nillore (NIL) and Quetta (QUE). Love and Rayleigh wave attenuation coefficients are estimated at periods of 15–100 s by taking their spectral amplitudes. Backus and Gilbert (1970) inversion theory is applied to obtain  $Q_\beta^{-1}$  models for the crust and upper mantle beneath the Bay of Bengal, the Arabian Fan, and the north and central Indian Ocean for different propagation paths. These studies will help im-

prove our knowledge of the tectonic process and temperature conditions prevailing under the Indian Ocean, which will further shed light on its evolution and tectonics.

## 2. Data analysis

The details of the earthquakes are listed in Table 1. The earthquake parameters have been taken from either International Seismological Centre (ISC) bulletins or National Oceanic and Atmospheric Administration (NOAA) tape file. The various wave propagation paths across the Bay of Bengal, Arabian Fan, and north and central Indian Ocean are shown in Fig. 1 and are listed in Table 2. The fundamental-mode Love and Rayleigh waves recorded at various Indian Seismograph and other WWSSN stations such as HOW, SHL, VIS, MDR, HYB, KOD, CHG, TRD, POO, BOM, GOA, NDI, NIL and QUE are analysed. Some of the signals used in the present study are shown in Fig. 2. The fundamental-mode surface waves are digitized at an irregular time interval using a digitizer and they are interpolated at a time interval of 0.25 s using the Lagrangian interpolation method. The long-period vertical component record is used in general for Rayleigh waves. However, some Indian seismic stations such as TRD, VIS, BOM and GOA have an intermediate period ( $T_0 = 8$  or  $12$  s) horizontal component only. In that case, the horizontal component record has been used for the Rayleigh wave. The north–south or east–west horizontal component which lies approximately perpendicular to the wave propagation path has been used for the Love wave. The linear trend and the arithmetic mean are removed from the digitized data. The data are tapered at both ends, and are then Fourier analysed using the FFT method to obtain the spectral amplitudes. These spectral data are corrected for the difference in seismic moment value for different earthquakes. For this purpose, spectra are normalized to an earthquake seismic moment of magnitude  $M = 5.5$ . The magnitude–moment relation given by Singh (1988a) has been used to normalize the seismic moment. Dissipation factor  $Q^{-1}$ , values for Love and Rayleigh

waves are estimated using the method of Burton (1974), with an extension to the earthquake source. In this method, the fault plane solution must be known. These solutions for the earthquakes listed in Table 1 have been taken from Banghar and Sykes (1969), Stein (1978), Stein and Okal (1978), Bergman and Solomon (1980, 1985), Bergman et al. (1984) and Singh (1988a). The earthquake which lies nearest to the known available focal mechanism solution has been considered as the representative fault plane solution for that particular earthquake. There are sufficient focal mechanism solutions available in the Indian Ocean to give the representative focal mechanism for the earthquakes listed in Table 1. If some error occurs because of an incorrect assumption of earthquake focal mechanism solution, this will be reflected in

the standard deviation of attenuation value. The spectral amplitudes are corrected for the instrumental effect (Ben-Menahem et al., 1968), the amplitudes are then corrected for the radiation pattern of the source (Ben-Menahem and Harkrider, 1964), and the values of  $Q^{-1}$  are estimated from the logarithmic form of the amplitude equation as described by Singh and Gupta (1979). The pertinent details of the earthquakes and various seismic stations used in this study are shown in Fig. 1 for 98 different paths. The logarithmic form of the amplitude equation is expressed as

$$A_f = K(E \sin \Delta)^{-1/2} \exp(-\pi E \Delta f / QU) \quad (1)$$

where  $A_f$  is the spectral amplitude at frequency  $f$  (in Hz),  $E$  is the radius of the Earth,  $\Delta$  is the distance (in km) from epicentre to the recording

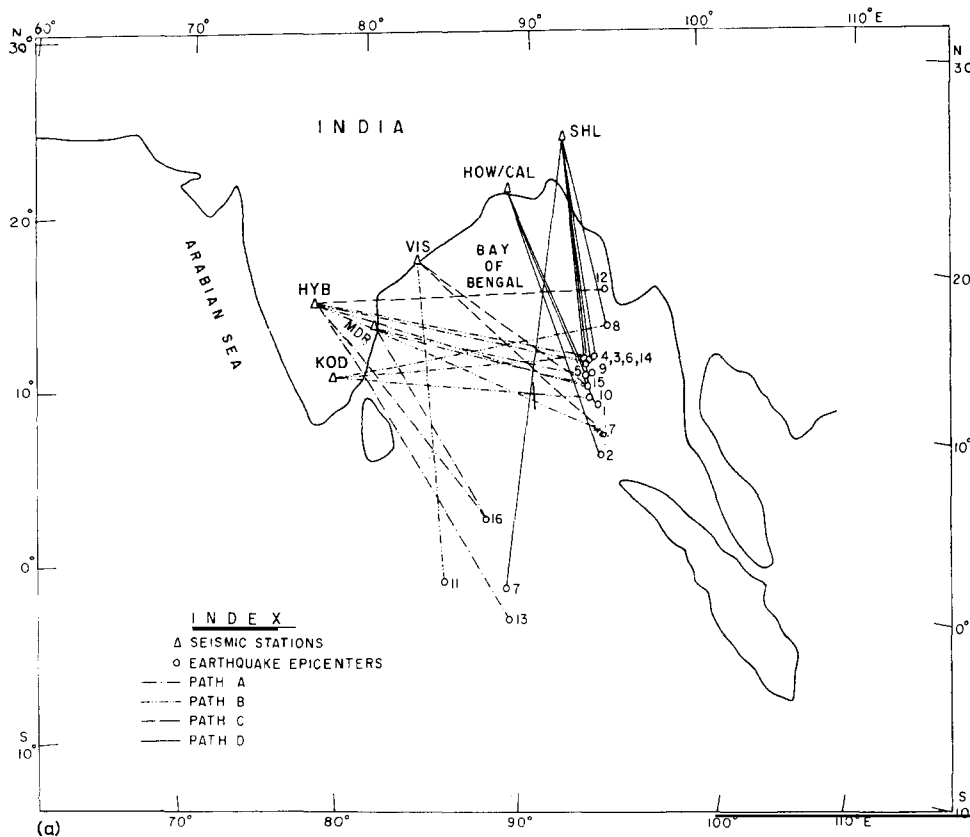


Fig. 1. Surface wave attenuation paths used in this study. (a) Bay of Bengal Fan, (b) Arabian Fan, and (c) north and central Indian Ocean. Recording stations are indicated by triangles and epicentres by circles.

station,  $K$  is a constant,  $Q$  is the dissipation factor at frequency  $f$  and  $U$  is the group velocity at frequency  $f$ .

The group velocities for the same propagation paths and regions have been determined in our earlier studies (Brune and Singh, 1986; Singh, 1988b,c). The same velocity models and group velocity values are considered for these regions.  $Q^{-1}$  values for Love and Rayleigh waves are shown in Fig. 3. After obtaining  $Q^{-1}$  values, the attenuation coefficients,  $\gamma$ , are estimated at time periods from 15 to 100 s using the relation

$$\gamma = \frac{\pi}{UTQ} \quad (2)$$

where  $T$  is the time period and  $U$  is the group velocity at  $T$  s. The Love and Rayleigh wave

attenuation coefficient values are shown in Fig. 4 and dissipation factor values are listed in Table 3.

### 3. Inversion of attenuation data

The frequency-dependent amplitude decay of surface wave data can be interpreted in terms of anelasticity vs. depth (Anderson and Archambeau, 1964). The application of surface wave attenuation studies has a number of advantages. The long-period surface wave reduces the complexities of source, instrument and path differences, and, because of its longer wavelength, the scattering and reflections are also minimized. Complexities as a result of the presence of low velocity zones are also minimized. In this way, surface wave

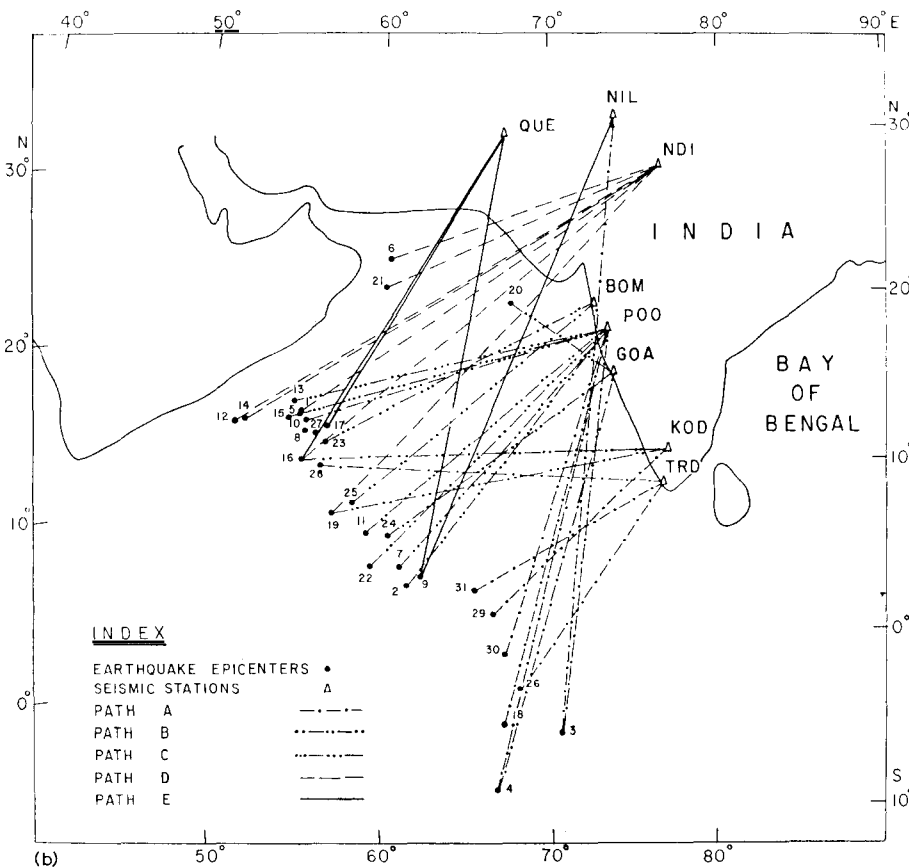


Fig. 1 (continued).

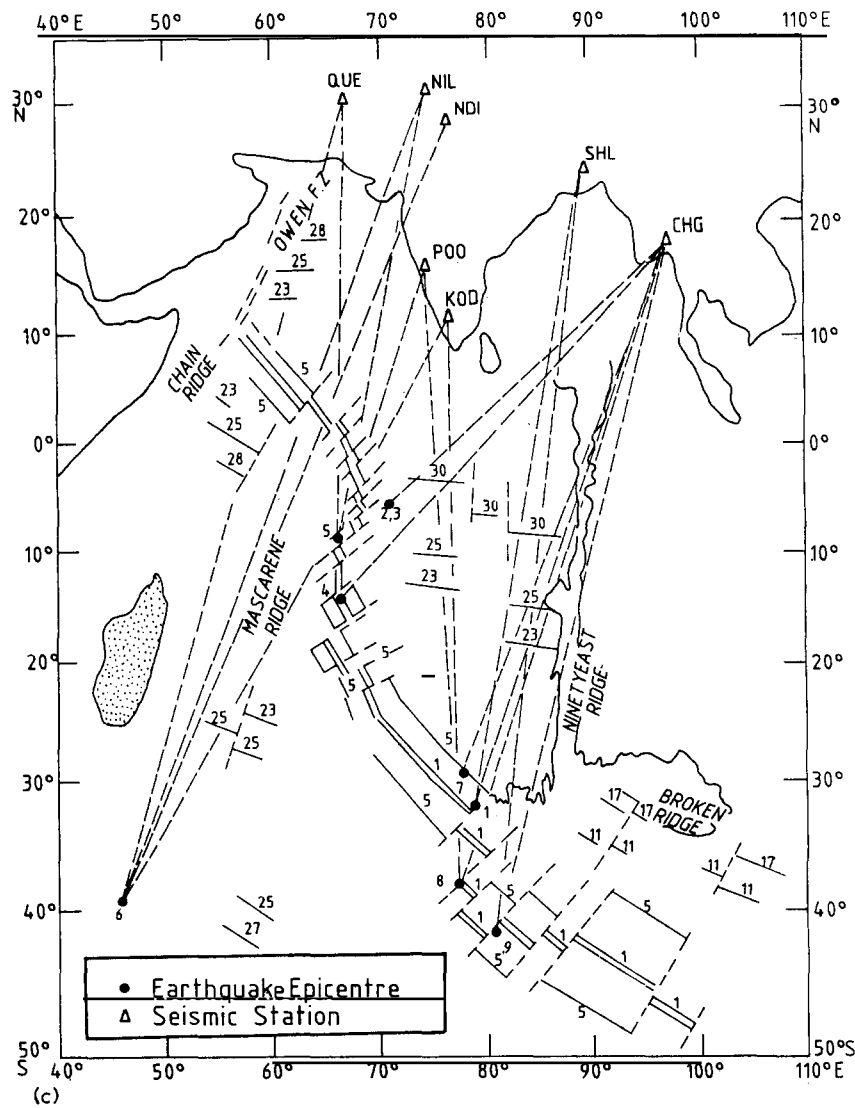


Fig. 1 (continued).

attenuation studies can give a better estimate of the material condition prevailing inside the earth. The shear wave dissipation,  $Q^{-1}$  of surface waves over a layered medium at a given period is equal to the sum of the dissipation in each layer, assuming  $Q^{-2}(Z)$  is smaller (Anderson and Archambeau, 1964). The surface wave attenuation coefficient values and their standard deviations at

different time periods can be used to obtain  $Q_{\beta}^{-1}(Z)$  models as a function of depth. Mitchell (1975) modified the relations given by Anderson et al. (1965) for calculating the attenuation of dispersed surface waves. The attenuation coefficients for Love and Rayleigh waves are related to the dissipation factors for P- and S-waves and the partial derivatives of Love and Rayleigh wave

TABLE 1

Parameters of earthquakes used in the present study for Love and Rayleigh wave attenuation studies

Sl. No.	Date	Origin time (UTC)	Epicentre		Magnitude	
			Lat. (deg)	Long. (deg E)	$m_b$	$M$
(A) Bay of Bengal Fan						
1	22 Nov. 1963	16:15:54.0	10.4 N	94.0	5.7	5.7
2	30 Nov. 1963	21:40:20.3	6.6 N	94.2	5.3	5.3
3	16 Sep. 1964	01:26:26.9	10.9 N	93.1	5.7	5.7
4	04 Apr. 1966	02:51:37.6	11.9 N	92.5	5.1	5.1
5	04 Sep. 1966	04:37:05.6	12.0 N	92.9	5.2	5.2
6	04 Sep. 1966	06:42:12.2	11.8 N	92.5	5.1	5.1
7	26 Apr. 1967	13:11:42.2	01.3 S	89.4	5.0	5.0
8	06 Sep. 1967	07:30:10.8	14.7 N	93.6	5.6	5.6
9	20 Dec. 1967	11:34:25.9	11.8 N	93.0	5.4	5.4
10	06 May 1970	15:21:55.1	9.8 N	92.9	5.3	5.1
11	03 Aug. 1978	01:10:26.3	0.9 S	84.3	5.6	5.5
12	03 Oct. 1979	11:35:12.5	18.1 N	94.8	5.6	4.9
13	28 Jan. 1980	14:46:39.3	3.4 S	88.9	5.4	5.2
14	02 Nov. 1981	21:10:26.8	12.2 N	92.9	5.7	5.5
15	16 Dec. 1982	08:56:35.5	11.7 N	92.9	5.4	—
16	21 Aug. 1983	12:06:48.0	3.2 N	87.5	5.2	—
17	17 Sep. 1983	04:40:36.4	7.9 N	93.2	5.3	—
(B) Arabian Fan						
1	19 Mar. 1964	09:42:36.0	14.4 N	56.4	5.8	—
2	18 Oct. 1964	09:06:26.0	02.9 N	65.7	6.8	—
3	12 Sep. 1965	22:02:34.3	06.5 S	70.8	6.2	—
4	05 Oct. 1965	09:44:29.6	09.1 S	67.3	5.1	—
5	27 Mar. 1966	01:40:59.5	14.4 N	56.7	5.1	—
6	30 Mar. 1966	04:18:38.3	21.8 N	62.2	5.5	—
7	28 Apr. 1966	18:08:55.2	4.2 N	62.8	5.0	—
8	18 Jul. 1966	09:59:09.8	13.0 N	57.5	5.0	—
9	15 Aug. 1966	10:20:42.8	3.8 N	64.0	5.8	6.2
10	14 Sep. 1966	00:47:05.0	14.5 N	56.4	5.0	—
11	03 Nov. 1966	21:43:10.3	6.6 N	60.4	5.1	—
12	25 Dec. 1966	05:42:45.9	14.2 N	53.7	5.2	—
13	15 Oct. 1967	06:36:39.7	14.7 N	56.4	5.1	—
14	08 Feb. 1968	12:28:21.0	14.6 N	54.0	5.4	—
15	30 Aug. 1968	22:02:19.8	14.6 N	56.3	5.2	—
16	29 Mar. 1969	13:49:04.0	10.4 N	56.8	5.6	5.6
17	22 Apr. 1969	22:34:38.4	12.8 N	58.3	5.7	—
18	22 Sep. 1969	01:40:20.8	5.6 S	68.2	5.1	—
19	14 Dec. 1969	18:37:09.5	8.2 N	58.5	5.9	—
20	26 Mar. 1975	16:19:19.7	19.8 N	68.4	5.2	—
21	19 May 1975	08:00:00.1	21.1 N	61.8	5.0	—
22	03 Jan. 1977	06:15:50.0	6.7 N	60.2	5.0	—
23	11 Jan. 1977	14:51:05.9	13.1 N	54.5	5.1	—
24	02 Jan. 1979	19:50:47.4	4.9 N	62.1	5.1	4.7
25	10 Mar. 1979	06:45:09.9	7.5 N	59.7	5.1	—
26	25 Dec. 1979	23:46:32.8	2.7 S	67.9	5.8	5.6
27	26 Jan. 1980	01:00:53.1	13.7 N	57.1	5.0	—
28	31 Aug. 1980	16:30:54.6	11.3 N	57.5	5.3	4.7
29	11 Dec. 1980	04:44:05.0	1.3 N	66.8	5.1	—
30	16 Jul. 1981	09:11:46.4	1.3 S	67.6	5.1	5.1
31	25 Oct. 1982	17:08:28.8	2.9 N	65.9	5.5	5.5

TABLE 1 (continued)

Sl. No.	Date	Origin time (UTC)	Epicentre		Magnitude	
			Lat. (deg)	Long. (deg E)	$m_b$	$M$
(C) North and central Indian Ocean						
1	19 Dec. 1965	22:06:32.8	32.2 S	78.8	5.5	–
2	11 Nov. 1967	18:00:00.7	6.1 S	71.4	5.4	5.7
3	02 Mar. 1968	22:02:24.8	6.1 S	71.4	5.5	–
4	25 Oct. 1970	12:00:35.2	13.7 S	66.3	5.6	5.9
5	06 Dec. 1972	05:31:44.8	9.2 S	67.3	5.6	–
6	08 Jan. 1974	21:47:21.6	39.0 S	46.2	5.9	6.1
7	02 Nov. 1976	07:13:15.7	29.3 S	77.7	5.8	6.5
8	22 Nov. 1976	04:46:26.0	38.5 S	78.6	5.1	–
9	19 Feb. 1977	07:53:23.6	41.3 S	80.5	5.8	6.0

phase velocities with respect to the shear and compressional wave velocities. These equations are expressed as follows:

$$\begin{aligned}\gamma_L &= \frac{\pi}{C_L T} \sum_{l=1}^N \left( \frac{\partial Q_L^{-1}}{\partial Q_{\beta l}} \right)_f Q_{\beta l}^{-1} \\ &= \frac{\pi}{T} \sum_{l=1}^N \left( \frac{\beta_l}{C_L^2} \frac{\partial C_L}{\partial \beta_l} \right)_{fd} Q_{\beta l}^{-1}\end{aligned}\quad (3)$$

$$\begin{aligned}\gamma_R &= \frac{\pi}{C_R T} \sum_{l=1}^N \left[ \left( \frac{\partial Q_R^{-1}}{\partial Q_{\alpha l}} \right) Q_{\alpha l}^{-1} + \left( \frac{\partial Q_R^{-1}}{\partial Q_{\beta l}} \right) Q_{\beta l}^{-1} \right] \\ &= \frac{\pi}{T} \left[ \sum_{l=1}^N \left( \frac{\alpha_l}{C_R^2} \frac{\partial C_R}{\partial \alpha_l} \right)_{fd\beta} Q_{\alpha l}^{-1} \right. \\ &\quad \left. + \sum_{l=1}^N \left( \frac{\beta_l}{C_R^2} \frac{\partial C_R}{\partial \beta_l} \right)_{fd\alpha} Q_{\beta l}^{-1} \right]\end{aligned}\quad (4)$$

where  $\alpha$  is the P-wave velocity,  $\beta$  is the S-wave velocity,  $C_L$  is the Love wave phase velocity,  $C_R$  is the Rayleigh wave phase velocity,  $l$  is a layer index,  $\gamma_L$  is the Love wave attenuation coefficient,  $\gamma_R$  is the Rayleigh wave attenuation coefficient,  $Q_\alpha$  is the P-wave dissipation factor,  $Q_\beta$  is the S-wave dissipation factor. The subscripts f,  $\alpha$ ,  $\beta$  and d refer to the frequency, compressional and shear wave velocities, and density, respectively, which are held constant. Partial derivatives of Love and Rayleigh wave phase velocities with respect to P- and S-wave velocities are computed (Harkrider, 1968). The velocity models for the above calculation have been taken from Brune

and Singh (1986) and Singh (1988b,c) for the same propagation paths and regions as in this study. Surface wave attenuation is more sensitive to the shear wave dissipation factor,  $Q_\beta$ , than to the compressional wave dissipation factor,  $Q_\alpha$ . For this reason, we have considered  $Q_\beta^{-1}$  values only for the inversion and  $Q_\alpha$  is assumed to be twice as large as  $Q_\beta$  at all depths (Anderson et al., 1965). The Backus and Gilbert (1970) inversion theory is applied to eqns. (3) and (4) in differential inverse as discussed by Hwang and Mitchell (1987). The inversion yields a model for  $Q_\beta^{-1}(Z)$  at different depths, with the resolving kernels. The selection of the final model is made by comparing the theoretical and observed attenuation coefficients for Love and Rayleigh waves which fit the observed values well for the data for both of the surface waves. The standard deviation of attenuation coefficient and its values are important input parameters in this inversion. The errors in surface wave attenuation determination may be caused by several reasons, such as the focusing and defocusing of surface waves from lateral variations in structure, higher-mode interference of Love wave with fundamental mode, geological complexities along the wave propagation path and coastline effect at the ocean–continent margin. These errors can be greatly reduced by considering a larger data set for the same propagation path. A large number of trial solutions are made for different values of variance. The variance is an adjustable parameter and is used to effect a trade-off between the resolution and the standard deviation of the model.

TABLE 2

Wave propagation paths at different seismic stations for Love and Rayleigh wave attenuation studies

Sl. No.	Epicentre		Seismic stations
	Lat. (deg)	Long. (deg E)	
<b>(A) Bay of Bengal Fan</b>			
1	10.4 N	94.0	HOW
2	6.6 N	94.2	HOW
3	10.9 N	93.1	HOW, MDR
4	11.9 N	92.5	SHL, KOD
5	12.0 N	92.9	KOD, SHL, HOW
6	11.8 N	92.5	KOD, SHL
7	01.3 S	89.4	KOD, SHL
8	14.7 N	93.6	KOD, SHL
9	11.8 N	93.0	SHL
10	9.8 N	92.9	KOD, SHL
11	0.9 S	84.3	VIS
12	18.1 N	94.8	HYB
13	3.4 S	88.9	HYB
14	12.2 N	92.9	HYB
15	11.7 N	92.9	VIS, HYB
16	3.2 N	87.5	MDR, HYB
17	7.9 N	93.2	VIS, HYB
<b>(B) Arabian Fan</b>			
1	14.4 N	56.4	NDI
2	02.9 N	65.7	POO
3	06.5 S	70.8	POO, NIL
4	09.1 S	67.3	POO
5	14.4 N	56.7	POO
6	21.8 N	62.2	NDI
7	4.2 N	62.8	POO
8	13.0 N	57.5	POO
9	3.8 N	64.0	POO, NDI, QUE, NIL
10	14.5 N	56.4	POO
11	6.6 N	60.4	POO
12	14.2 N	53.7	POO
13	14.7 N	56.4	POO
14	14.6 N	54.0	NDI, POO
15	14.6 N	56.3	POO
16	10.4 N	56.8	QUE, NDI, KOD, POO
17	12.8 N	58.3	POO, KOD, NDI
18	5.6 S	68.2	POO
19	8.2 N	58.5	NDI, KOD, NIL
20	19.8 N	68.4	GOA, BOM
21	21.1 N	61.8	NDI
22	6.7 N	60.2	BOM, GOA
23	13.1 N	54.5	BOM
24	4.9 N	62.1	BOM, GOA, POO
25	7.5 N	59.7	BOM, GOA
26	2.7 S	67.9	GOA, TRD, KOD
27	13.7 N	57.1	TRD
28	11.3 N	57.5	TRD, GOA
29	1.3 N	66.8	KOD

TABLE 2 (continued)

Sl. No.	Epicentre		Seismic stations
	Lat. (deg)	Long. (deg E)	
<b>(B) Arabian Fan</b>			
30	1.3 S	67.6	POO
31	2.9 N	65.9	TRD
<b>(C) North and central Indian Ocean</b>			
1	32.2 S	78.8	CHG, POO, NIL
2	6.1 S	71.4	NIL, POO
3	6.1 S	71.4	CHG, NDI, NIL, POO
4	13.7 S	66.3	CHG
5	9.2 S	67.3	POO, QUE, NDI, NIL
6	39.0 S	46.2	CHG, NIL, QUE, NDI, KOD, POO
7	29.3 S	77.7	CHG
8	38.5 S	78.6	CHG, SHL, KOD, POO
9	41.3 S	80.5	SHL

A higher variance value increases the resolution but produces a larger standard deviation value for the model and vice versa. The standard deviation of the resulting models can thus be improved by subdividing the layers of the selected velocity model. The layer thickness of the selected velocity model is further subdivided into a number of layers of 2–5 km thickness, keeping the same layer parameters P- and S-velocities and density. Figure 5 shows the models resulting from these inversions and the standard deviation of the model at each subdivided layer. These models give a fairly good fit to both Rayleigh and Love wave attenuation data (Fig. 4). The resolving kernels for these inversions are shown in Fig. 6 at a few depths for some selected regions. Narrow and sharp peaks at the appropriate depth section indicate a high degree of resolution, whereas broad peaks mean poor resolution. The resolving kernels indicate that the resolution is good only up to 100 km depth and then deteriorates.

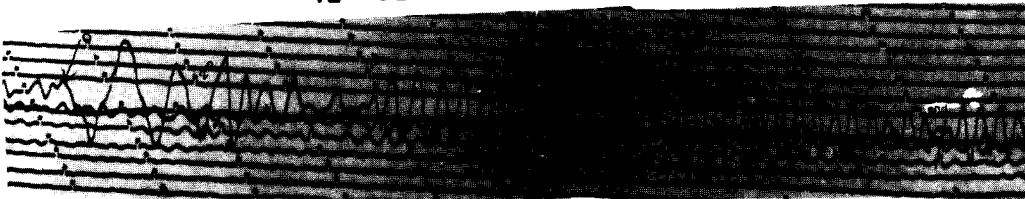
#### 4. Discussion

Figure 4 shows the large standard deviation for surface wave attenuation coefficient values which may be a result of the observed error and/or the presence of heterogeneities in the crust and upper

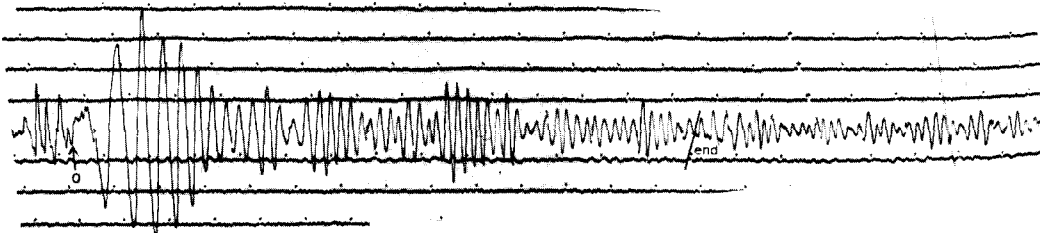
15 AUG. 1966 NDI (Z)



12 SEPT. 1965 NIL (Z)



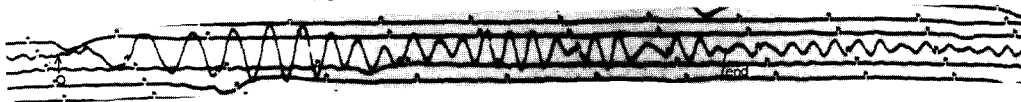
22 APRIL 1969 QUE (Z)



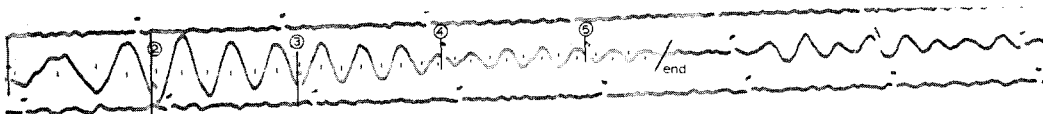
6 MAY 1970 SHL (Z)



15 AUG. 1966 NIL (Z)



16 JAN. 1966 KOD (Z)



22 APR. 1969 P00 (Z)

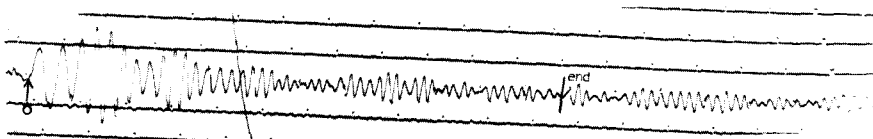


Fig. 2. Typical seismograms recorded at various seismic stations.

TABLE 3

Love and Rayleigh wave attenuation data for the Bay of Bengal, the Arabian Fan, and the north and central Indian Ocean

Time period (s)	Bay of Bengal		Arabian Fan, paths A, B, C		Arabian Fan, paths D, E		North and central Indian Ocean			
							Off Ninetyeast Ridge		Across Ninetyeast Ridge	
	$Q_L^{-1}$	$Q_R^{-1}$	$Q_L^{-1}$	$Q_R^{-1}$	$Q_L^{-1}$	$Q_R^{-1}$	$Q_L^{-1}$	$Q_R^{-1}$	$Q_L^{-1}$	$Q_R^{-1}$
15	0.0036	0.0046	0.0058	0.0078	0.0058	0.0074	0.0043	0.0067	0.0029	0.0032
20	0.0067	0.0063	0.011	0.0112	0.0106	0.0121	0.0073	0.0072	0.004	0.0042
25	0.004	0.0047	0.0157	0.0158	0.0081	0.0093	0.0086	0.0096	0.0071	0.0047
30	0.004	0.0051	0.0082	0.0141	0.0089	0.0061	0.011	0.0091	0.0031	0.0054
35	0.0043	0.0057	0.0103	0.011	0.0043	0.0061	0.015	0.012	0.0034	0.0016
40	0.0026	0.0029	0.0144	0.011	0.0056	0.0067	0.01	0.012	0.0026	0.0019
45	0.0024	0.0033	0.01	0.011	0.0072	0.0088	0.0125	0.0099	0.0036	0.0028
50	0.0068	0.0037	0.0095	0.011	0.0122	0.0087	0.0136	0.0087	0.0027	0.0037
55	0.0023	0.0021	0.0046	0.0083	0.0076	0.0138	0.015	0.01	0.003	0.0041
60	0.0067	0.0061	0.0084	0.0046	0.0033	0.0099	0.021	0.0152	0.0042	0.0053
65	0.0055	0.0082	0.0073	0.0099	0.0128	0.0099	0.0183	0.0058	0.0055	0.0041
70	0.0099	0.0036	0.0139	0.0089	0.0059	0.0071	0.0148	0.0134	0.0059	0.0053
75	0.0053	0.0038	0.0096	0.0115	0.0053	0.0096	0.0106	0.0057	0.0053	0.0096
80	0.0114	0.0031	0.0137	0.0102	0.0046	0.01	0.0057	0.0041	0.0091	0.0051
85	0.0073	0.0033	0.0133	0.0087	0.0158	0.0173	0.012	0.016	0.0049	0.0053
90	0.0129	0.0034	0.022	0.0138	0.0116	0.0138	0.0129	0.0138	0.0039	0.0057
95	0.0082	0.011	0.0245	0.0133	0.0136	0.0169	0.0082	0.0048	0.0055	0.0048
100	0.0143	0.0089	0.0287	0.0153	0.0187	0.0127	0.0057	0.0051	0.0029	0.0076

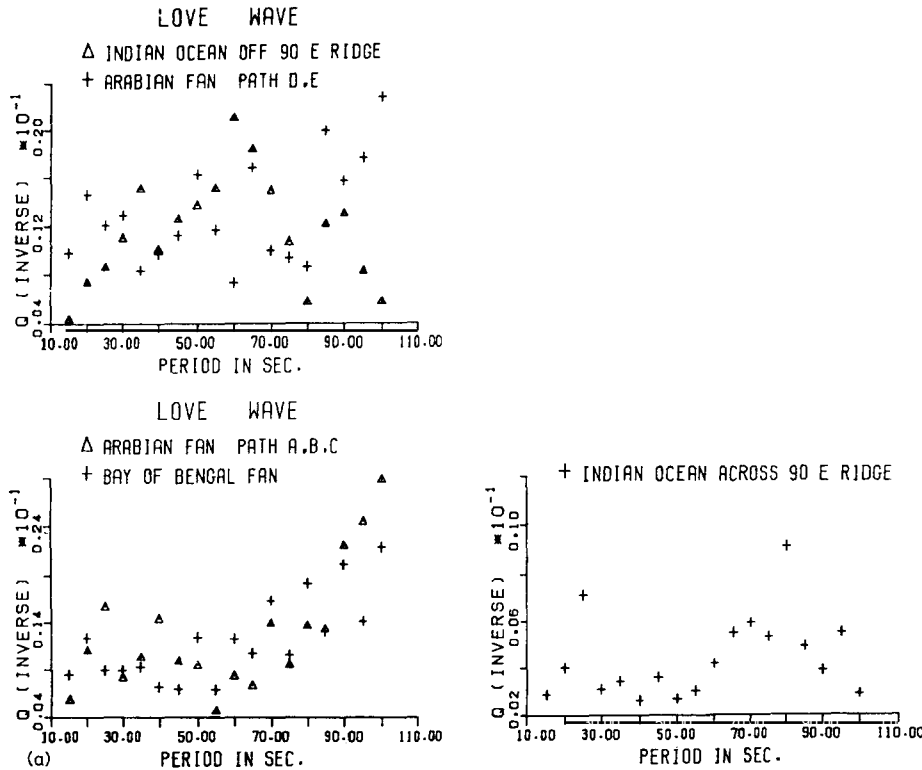


Fig. 3. Observed Love (a) and Rayleigh (b) wave  $Q^{-1}$  data for the Bay of Bengal, the Arabian Fan, and the north and central Indian Ocean.

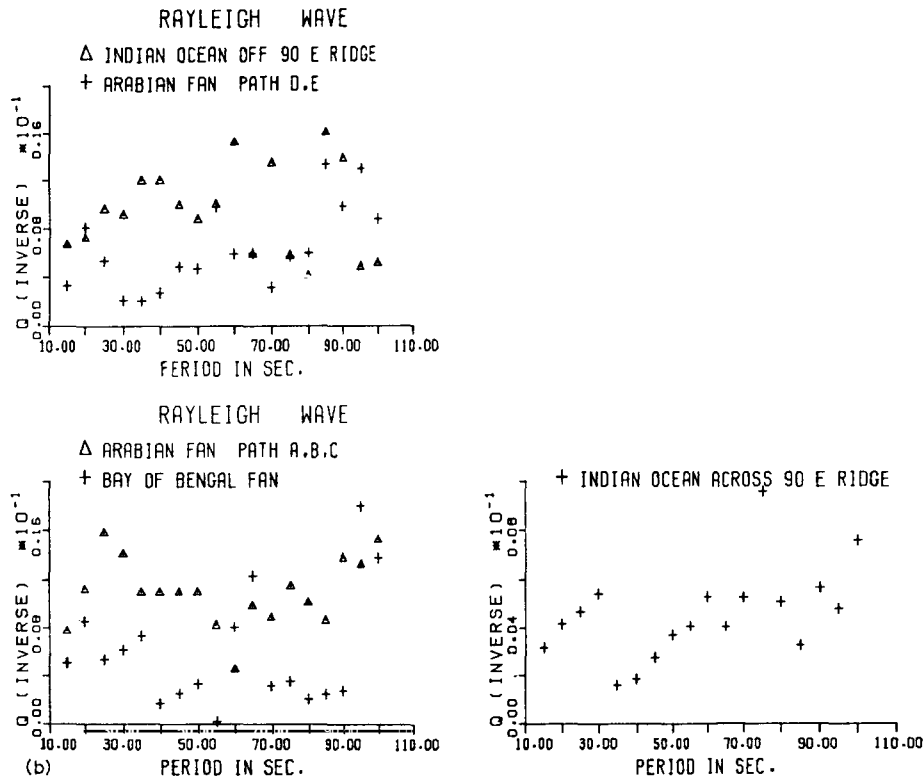


Fig. 3 (continued).

mantle beneath the Indian Ocean. We have not considered errors caused by reflection and refraction losses and mode conversion effects. As these errors are small and systematic, compared with the estimates of standard deviation for surface wave attenuation values, they can be neglected. Figure 5 shows the  $Q_{\beta}^{-1}$  models for the Bay of Bengal, the Arabian Fan, and the Indian Ocean off Ninetyeast Ridge and across Ninetyeast Ridge. In the Arabian Fan, paths A, B and C correspond to pure oceanic structure with very little continental structure, whereas paths D and E are contaminated by slightly more continental structure. In all the  $Q_{\beta}^{-1}$  models, we find a higher attenuation zone below Moho depth.  $Q_{\beta}^{-1}$  models in Fig. 5 for the Bay of Bengal Fan, the Arabian Fan sediments, and the Indian Ocean across Ninetyeast Ridge and off Ninetyeast Ridge show a higher attenuation zone in the asthenosphere than in the lithosphere. The high attenuating zone in the Bay of Bengal Fan at a depth of 120 km may

be because of higher temperature. The increase in hydrostatic pressure as a result of the load exerted by a large sedimentary column and the horizontal stress caused by the collision of Indian and Eurasian plates has given rise to adiabatic heating and increase in temperature at this depth. In the asthenosphere  $Q_{\beta}^{-1}$  values are larger (approximately by a factor of two) than those of the lithosphere beneath the Arabian Fan. Lithosphere-asthenosphere boundary is defined as the depth at which there is a significant increase in  $Q_{\beta}^{-1}$  value and this reaches a maximum in the asthenosphere. The lithosphere thickness is estimated to be 120 km for the Bay of Bengal Fan; 70 km for the Arabian Fan; 80 km for the Indian Ocean across Ninetyeast Ridge and 100 km for the Indian Ocean off Ninetyeast Ridge, respectively. The lower lithospheric thickness in the Arabian Fan shows that the region may be in the transition zone between continental and oceanic structure. Indian lithosphere has become thin be-

neath the Arabian Fan. In the upper mantle, below Moho (60 km from the surface) there seems to be high temperature, which has given rise to a high-attenuation zone. In general, such a zone is associated with higher temperature than the normal value expected at that depth. The subduction of the Arabian plate beneath the southern coast of Pakistan, as suggested by Quittmeyer and Kafka (1984), might have increased the temperature below Moho depth in this region. Gaynanov (1980) found a large negative gravity anomaly over the

Arabian-Indian Ridge, which was explained by assuming a low subcrustal substance, identified as asthenosphere, whose top occurs a mere 7-9 km beneath the rift valley. Taylor (1968) conducted a total magnetic intensity survey across the north Arabian Sea and found two sub-linear magnetic trends across this region. He interpreted this magnetic anomaly as being the result of a linear tectonic feature which has been subsequently buried by the great volume of sediment that forms the Indus River cone. Further, Taylor (1968) stated

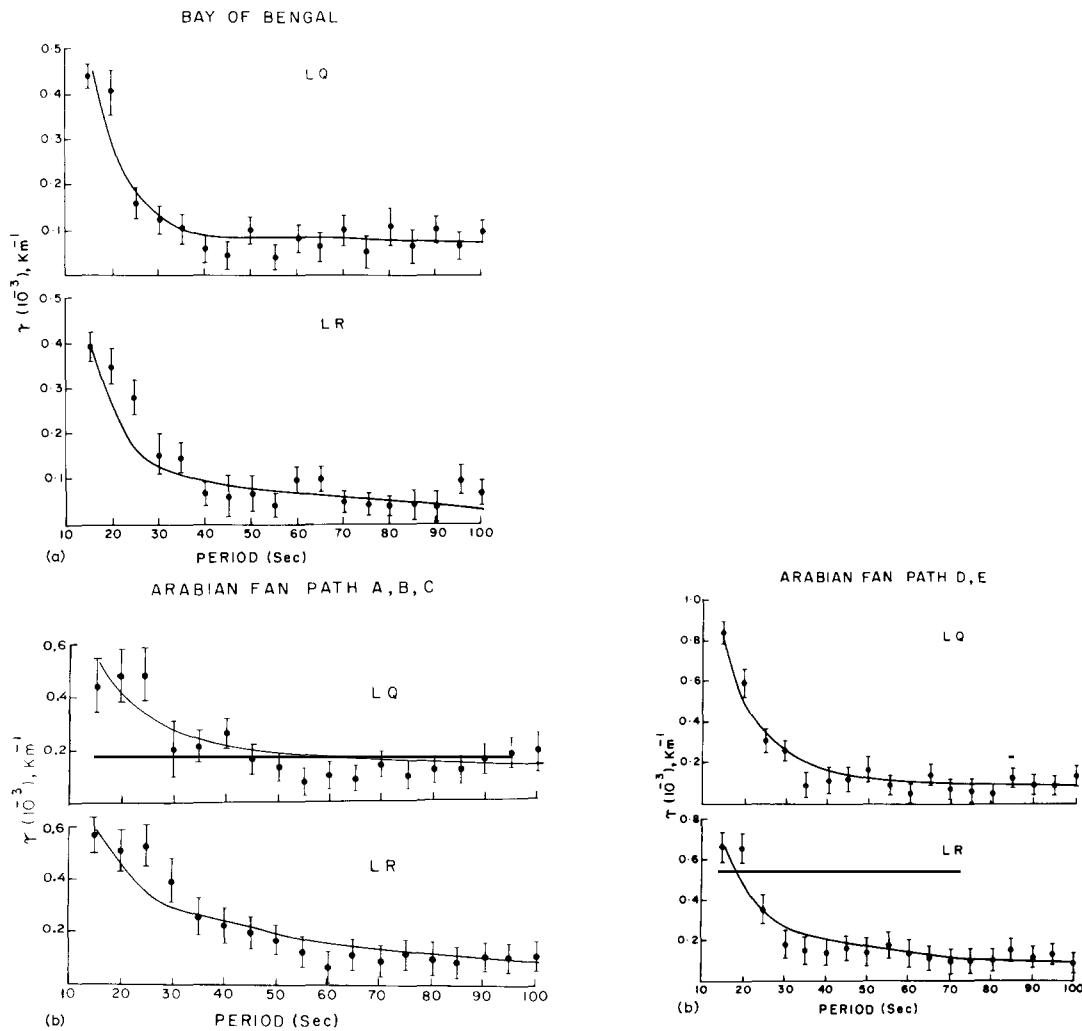


Fig. 4. Comparison of observed attenuation coefficients (dots), and 95% confidence limits for (a) Bay of Bengal Fan, (b) Arabian Fan, (c) north and central Indian Ocean, with the theoretical value (continuous line) corresponding to the models derived from the separate inversion of Love and Rayleigh wave attenuation data.

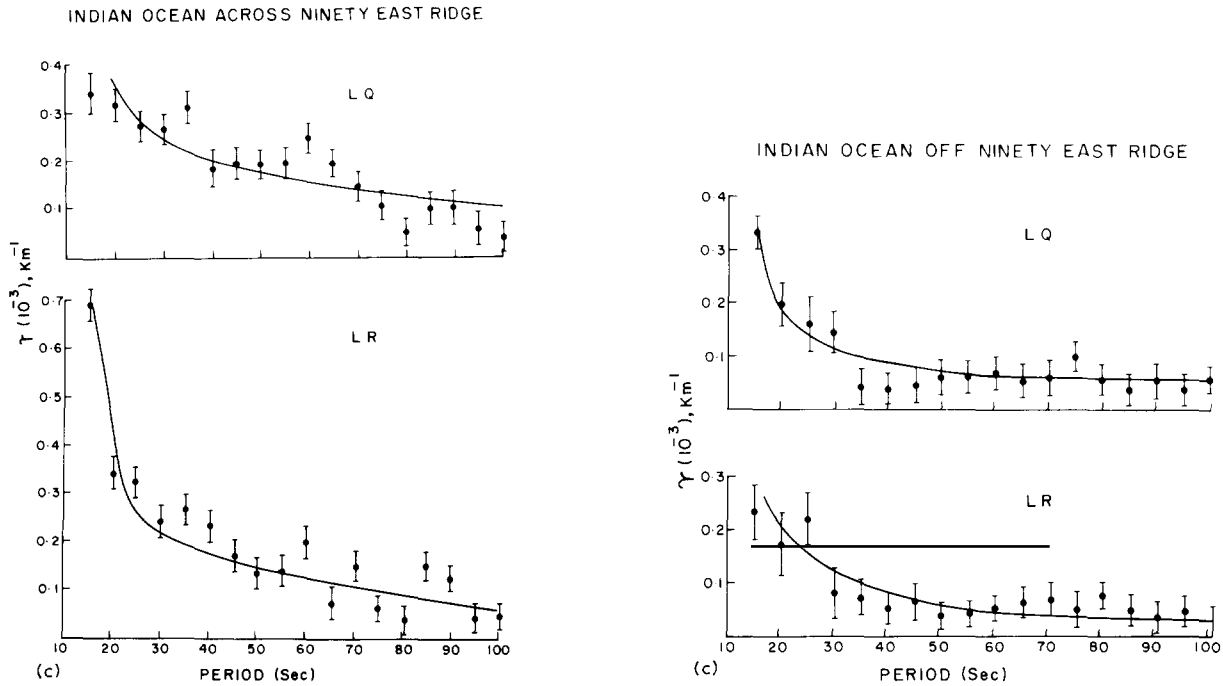


Fig. 4 (continued).

that this ridge-like feature could be related to the Murray Ridge and/or linked to the northern end of the Chagos–Laccadive Plateau.

The  $Q$ -structure beneath the central Indian Ocean obtained in this study represents the average picture for a lithospheric age of 60–70 Ma old. The younger lithosphere ( $\sim 10$  Ma) constitutes less than  $\sim 10\%$  of the total path traversed (Fig. 1c) and we can assume that the anomalous effect of this young slow lithosphere does not greatly influence our observed attenuation values. Thus, the  $Q_{\beta}^{-1}$  models are representative of the older portion of the central Indian Ocean crust and upper mantle. The relatively thin lithosphere (80 km) across Ninetyeast Ridge compared with that off Ninetyeast Ridge of the Indian Ocean (100 km) suggests that a higher-temperature zone exists beneath the Ninetyeast Ridge axis at much shallower depth than off Ninetyeast Ridge. This result favours the geothermal model proposed by Forsyth (1975), which states that with an increase in age of the sea floor, the lithosphere thickness increases and reaches 70 km for ages of 30–40 Ma. Singh (1988b) has found the depth of the

low-velocity zone (LVZ) to be 78 km from the surface, and high temperature ( $1100\text{--}1200^{\circ}\text{C}$ ) is associated with this LVZ. Our study also finds that the high-attenuation zone starts at this shallow depth (80 km). Brune and Singh (1986) have estimated a 100 km thick LVZ at a depth of 74 km from the water surface beneath the Bay of Bengal Fan sediments using surface wave dispersion data.  $Q_{\beta}^{-1}$  models in Fig. 5(a) show a high-attenuation zone at a depth  $> 120$  km from the water surface. Similarly, a 100 km thick LVZ has been estimated at 64 km depth from the water surface beneath the Arabian Fan sediments by Singh (1988c), using surface wave dispersion data.  $Q_{\beta}^{-1}$  models in Fig. 5(b) show a high-attenuation zone at a depth of 60–160 km from the water surface. The high-attenuation zone estimated in the present study agrees well with the LVZ from surface wave dispersion studies by Brune and Singh (1986) and Singh (1988b,c). The lithosphere–asthenosphere boundary is not at the same depth as the top of LVZ for the Bay of Bengal Fan and the Indian Ocean off Ninetyeast Ridge. The Arabian Fan and the Indian Ocean across Ninetyeast Ridge

show approximately the same depth for the top of LVZ and the lithosphere–asthenosphere boundary. The lithosphere thickness estimated in this study for off Ninetyeast Ridge agrees well and is of a

similar order to that determined by Singh (1982) for the oceanic path of Eurasian continent.

$Q_{\beta}^{-1}$  models for the East Pacific Rise (< 10 Ma), Nazca Plate (~ 40 Ma) and Mid-Atlantic

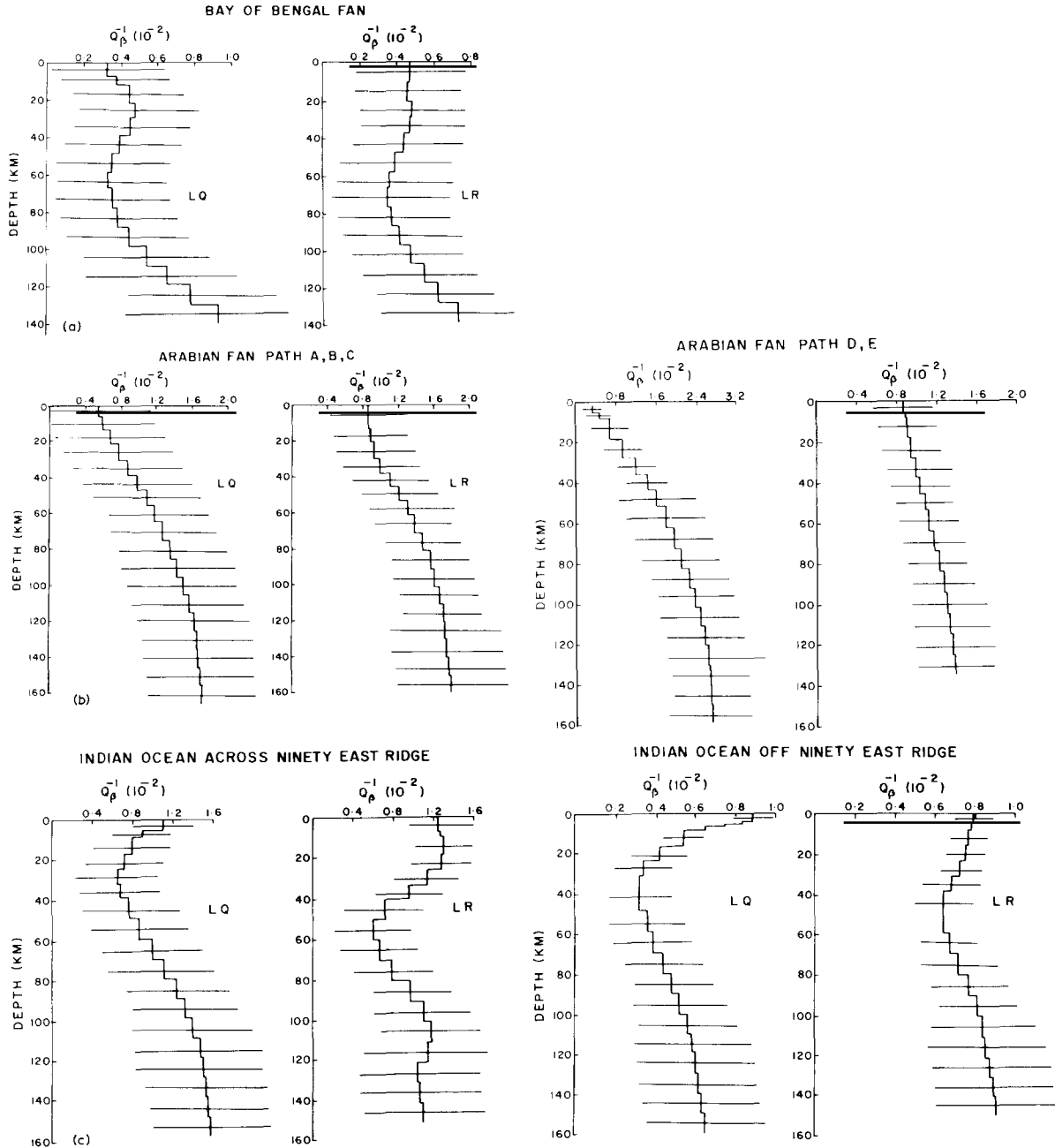


Fig. 5. Models resulting from the separate inversion of Love and Rayleigh wave attenuation data, and the standard deviation of the model (horizontal bars), for each layer.

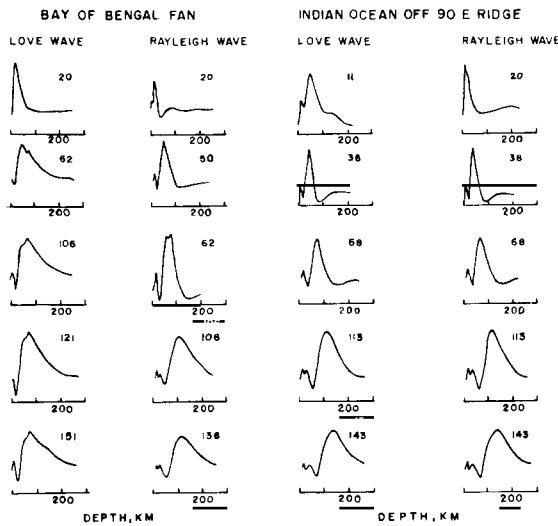


Fig. 6. Resolving kernels at a few depths for the selected models appearing in Fig. 5 for two regions. Depth is indicated at the right-hand side of the figure. The kernels have been normalized to the same maximum value for the display.

Ridge (0–23 Ma) are compared in Fig. 7 with the models obtained in this study. It can be seen that the highest values of  $Q_{\beta}^{-1}$  occur in the youngest region (East Pacific Rise, < 10 Ma in age), inter-

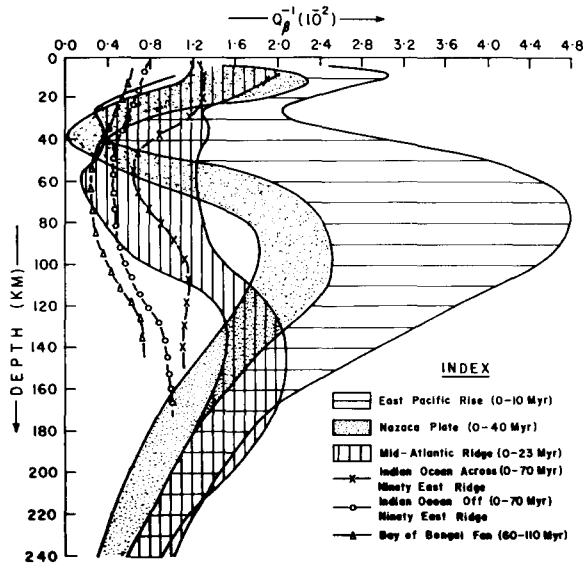


Fig. 7. Comparison of  $Q_{\beta}^{-1}$  models in this study with Atlantic and Pacific path inferred from Rayleigh wave data (Canas and Mitchell, 1978, 1981; Canas et al., 1981). The age of the ocean floor is given as an index.

mediate values in the Nazca Plate (0–40 Ma) and then in the Mid-Atlantic Ridge (0–23 Ma), as given by Canas et al. (1981). In this study,  $Q_{\beta}^{-1}$  values are lower for the Indian Ocean (0–70 Ma), the Arabian Fan (0–70 Ma) and the Bay of Bengal Fan (60–110 Ma) compared with the East Pacific Rise, Nazca Plate and Mid-Atlantic Ridge, which are younger (0–40 Ma). Our observed  $Q_{\beta}^{-1}$  values are in the same range as those for the older Pacific and Atlantic Oceans (50–100 Ma). The East Pacific Rise, Nazca Plate and Mid-Atlantic Ridge show a clear low- $Q$  zone, which extends to a depth of ~ 200 km. In the East Pacific Rise, the low- $Q$  zone is thicker than in the Nazca Plate, Mid-Atlantic Ridge, Indian Ocean and Bay of Bengal Fan. In this study, the low- $Q$  zone is centred at a depth of 80–160 km beneath the Indian Ocean across the Ninetyeast Ridge and similarly at 100–160 and 120–160 km for the Indian Ocean off Ninetyeast Ridge and the Bay of Bengal Fan, respectively.  $Q_{\beta}^{-1}$  models in this study support the hypothesis of Canas and Mitchell (1978, 1981) and Canas et al. (1981), which states that with an increase in the age of ocean floor, there is an increase in the lithospheric thickness, and the  $Q_{\beta}^{-1}$  value (low- $Q$  zone) becomes smaller and less pronounced.

**Acknowledgements**

I thank Dr. H.N. Srivastava, Director, Seismology, India Meteorological Department, New Delhi, for giving permission to use the seismograms in this study. I am grateful to Prof. Brian J. Mitchell of Saint Louis University for the critical review of this manuscript and providing the computer program to invert the surface wave attenuation data. I also wish to thank the Director, National Geophysical Research Institute, Hyderabad, for granting permission to publish this work.

**References**

Anderson, D.L. and Archambeau, C.B., 1964. The anelasticity of the Earth. *J. Geophys. Res.*, 69: 2071–2084.

- Anderson, D.L., Ben-Menahem, A. and Archambeau, C.B., 1965. Attenuation of seismic energy in the upper mantle. *J. Geophys. Res.*, 70: 1441–1449.
- Backus, G. and Gilbert, F., 1970. Uniqueness in the inversion of gross earth data, *Philos. Trans. R. Soc. London, A*, 266: 123–192.
- Banghar, A.R. and Sykes, L.R., 1969. Focal mechanism of earthquakes in the Indian Ocean and adjacent regions. *J. Geophys. Res.*, 74: 632–649.
- Ben-Menahem, A. and Harkrider, D.G., 1964. Radiation pattern of seismic surface waves from buried dipolar point source in a flat stratified Earth. *J. Geophys. Res.*, 69: 2605–2620.
- Ben-Menahem, A., Jarosch, H. and Rosenman, M., 1968. Large scale processing of seismic data in search of regional and global stress pattern. *Bull. Seismol. Soc. Am.*, 58: 1899–1932.
- Bergman, E.A. and Solomon, S.C., 1980. Oceanic intraplate earthquakes: implications for local and regional intraplate stress. *J. Geophys. Res.*, 85: 5389–5410.
- Bergman, E.A. and Solomon, S.C., 1985. Earthquake source mechanisms from body waveform inversion and intraplate tectonics in the northern Indian Ocean. *Phys. Earth Planet. Inter.*, 40: 1–23.
- Bergman, E.A., Nabelck, J.I. and Solomon, S.C., 1984. An extensive region of off-ridge normal faulting earthquakes in the southern Indian Ocean. *J. Geophys. Res.*, 89: 2425–2443.
- Brune, J.N. and Singh, D.D., 1986. Continent-like crustal thickness beneath the Bay of Bengal sediments. *Bull. Seismol. Soc. Am.*, 76: 191–203.
- Burton, P.W., 1974. Estimation of  $Q^{-1}$  from seismic Rayleigh waves. *Geophys. J.R. Astron. Soc.*, 36: 167–189.
- Canas, J.A. and Mitchell, B.J., 1978. Lateral variation of surface anelastic attenuation across the Pacific. *Bull. Seismol. Soc. Am.*, 68: 1637–1650.
- Canas, J.A. and Mitchell, B.J., 1981. Rayleigh wave attenuation and its variation across the Atlantic Ocean. *Geophys. J.R. Astron. Soc.*, 67: 159–176.
- Canas, J.A., Mitchell, B.J. and Correig, A.M., 1981.  $Q^{-1}$  models for the East Pacific Rise and the Nazca Plate. In: P.A. Davies and S.K. Runcorn (Editors), *Mechanisms of Plate Tectonics and Continental Drift*. Academic Press, London, pp. 123–133.
- Capon, J., 1971. Comparison of Love and Rayleigh wave multi-path propagation at LASA. *Bull. Seismol. Soc. Am.* 61: 1327–1344.
- Forsyth, D.W., 1975. The early structural evolution and anisotropy of the oceanic upper mantle. *Geophys. J.R. Astron. Soc.*, 43: 103–162.
- Gaynanov, A.G., 1980. *Gravimetricheskiye issledovaniya zemnyakory okeanov* (Gravimetric Investigations of the Oceanic Crust). Moscow University, 240 pp.
- Harkrider, D.G., 1968. The perturbation of Love wave spectra. *Bull. Seismol. Soc. Am.*, 58: 861–880.
- Hwang, H.J. and Mitchell, B.J., 1987. Shear velocities,  $Q$ , and the frequency dependence of  $Q$  in stable and tectonically active regions from surface wave observations. *Geophys. J. R. Astron. Soc.*, 90: 575–613.
- McGarr, A., 1969. Amplitude variations of Rayleigh waves—horizontal refractions. *Bull. Seismol. Soc. Am.*, 59: 1307–1334.
- Mitchell, B.J., 1975. Regional Rayleigh wave attenuation in North America. *J. Geophys. Res.*, 80: 4904–4915.
- Quittmeyer, R.C. and Kafka, A.L., 1984. Constraint on plate motions in southern Pakistan and northern Arabian Sea from the focal mechanism of small earthquakes. *J. Geophys. Res.*, 89: 2444–2458.
- Singh, D.D., 1982. Anelasticity of the crust and upper mantle beneath the Eurasian continent and nearby regions from the inversion of Love and Rayleigh wave attenuation data. *Geophys. J.R. Astron. Soc.*, 71: 751–774.
- Singh, D.D., 1988. Strain deformation in northern Indian Ocean. *Mar. Geol.*, 79: 105–118.
- Singh, D.D., 1988. Crust and upper mantle velocity beneath north and central Indian Ocean from the phase and group velocity of Rayleigh and Love waves. *Phys. Earth Planet. Inter.* 50: 230–239.
- Singh, D.D., 1988. Quasicontinental–oceanic structure beneath the Arabian Fan sediments from the observed surface wave dispersion studies. *Bull. Seismol. Soc. Am.*, 78: 1510–1521.
- Singh, D.D. and Gupta, H.K., 1979. Source mechanism and surface wave attenuation studies for Tibet earthquake of July 14, 1973. *Bull. Seismol. Soc. Am.*, 69: 737–750.
- Stein, S., 1978. An earthquake swarm on the Chagos Laccadive Ridge and its tectonic implications. *Geophys. J.R. Astron. Soc.*, 55: 577–588.
- Stein, S. and Okal, E.A., 1978. Seismicity and tectonics of the Ninetyeast Ridge area: evidence for internal deformation of the Indian Plate. *J. Geophys. Res.*, 83: 2233–2246.
- Taylor, P.T., 1968. Interpretation of north Arabian Sea aeromagnetic survey. *Earth Planet. Sci. Lett.*, 4: 232–236.